Acta Cryst. (1995). A51, 329–335

A Computer Simulation Approach for the Calculation of Diffuse Intensity Distributions from Crystals Undergoing the 2*H* to 6*H* Transformation by Layer Displacement Mechanism

BY V. K. KABRA AND DHANANJAI PANDEY

School of Materials Science and Technology, Banaras Hindu University, Varanasi-221 005, *India*

(*Received* 19 *September* 1994; *accepted* 11 *October* 1994)

Abstract

Limitations of the Markovian chain approach for the calculation of diffuse intensity distributions from crystals undergoing the 2*H* to 6*H* transformation by non-random insertion of layer displacement faults are pointed out. A computer simulation approach for the numerical computation of the diffuse intensity disributions in such situations is presented. The numerically computed intensity distributions along diffuse streaks, obtained by taking Fourier transforms of the pair correlations determined from simulated configuration corresponding to the intermediate states of transformation, show marked departures from those obtained analytically using the Markovian chain approach. Explanations for this discrepancy are advanced.

1. Introduction

The crystal structure of a large number of materials can be described in terms of stacking of layers of atoms in a close-packed manner (Pandey & Krishna, 1982, 1983). These layers can restack themselves on thermal annealing or mechanical deformation, leading to structural transformations involving change of stacking sequence and periodicity. Such restacking transformations have been the subject of investigation in a large number of metallic (Frey & Boysen, 1981; Hitzenberger, Karnthaler & Korner, 1985; Ahlers & Pelegrina, 1992; Nikolin, Babkevich, Izdkovskaya & Petrova, 1993; Demin, Nekrasov & Ustinov, 1993; Cardellini & Mazzone, 1993) and non-metallic materials (Jagodzinski, 1971; Krishna & Marshall, 1971*a*,*b*; Jepps & Page, 1980; Ogbuji, Mitchell & Heuer, 1981; Minagawa, 1978; Sebastian, Pandey & Krishna, 1982), and more recently in fullerenes (Muto, Van Tendeloo & Amelinckx, 1993). The restacking of layers during such transformations is brought about by a non-random insertion of stacking faults as confirmed by the appearance of characteristic diffuse streaks on single-crystal X-ray diffraction patterns taken from transforming crystals. From a theoretical analysis of the observed intensity distribution along streaked reciprocal-lattice rows in terms of physically plausible models for the statistical insertion of stacking faults, it is possible to determine the distribution and geometrical nature of stacking faults, which are generally characteristic of the transformation mechanism (Pandey, 1976; Pandey, Lele & Krishna, 1980*a*,*b*,*c*; Pandey & Lele, 1986, Pandey, Kabra & Lele, 1986; Kabra, Pandey & Lele, 1986). This diffraction approach for studying the mechanism of transformation between layer stackings was first developed in relation to the 2*H* to 6*H* transformation in SiC (Pandey *et al.*, 1980*a*,*b*). As pointed out by Pandey *et al.* (1980*a*), the 2*H* to 6*H* transformation in SiC by a layer displacement mechanism requires occurrence of layer displacement faults at three-layer separations as shown below:

Initial 2*H* structure: $\cdots A\ B\ \boxed{A}\ B\ A\ \boxed{B}\ A\ B\ \boxed{A}\ B\ A\ \boxed{B}\cdots$

Resulting 6*H* structure: $\cdots A\ B\ \boxed{C}\ B\ A\ \boxed{C}\ A\ B\ \boxed{C}\ B\ A\ \boxed{C}\cdots.$

The model employed by Pandey *et al.* (1980*a*) for the calculation of intensity distributions along the diffuse streaks is based on the assumption that the faults are inserted sequentially into a stack of layers from one end of the stack, as in any Markovian chain approach. The sequential fault probability for the layer displacement faults bringing about the 2*H* to 6*H* transformation is the probability of occurrence of such a fault with the next two layers not faulted (*i.e.* faults maintain a minimum separation of three layers), as one performs a random walk from one end of the stack towards the other. This model allows faulting of one third of the layers on the completion of the 2*H* to 6*H* transformation when the sequential fault probability becomes unity.

In real situations, the transformation can start anywhere in the crystal rather than sequentially from one end of the crystal. Unlike the sequential model, the independently formed 6*H* regions in different parts of the crystal may grow on both sides and eventually impinge on the neighbouring transformed regions. This impingement may either lead to the merger of the two 6*H* domains or to an interface, depending on whether the spacing between the neighbouring layer displacement faults in the two domains is of three or more layers. The formation of interfaces due to the occurrence of layer displacement faults at four or five layer separations leads to the arrest of the transformation because of the requirement of a minimum separation of three layers between contiguous faults. Kabra, Pandey & Lele (1988)

employed the Monte Carlo technique using integer pseudo-random numbers for the insertion of layer displacement faults in a pre-existing stack of layers with $2H$ structure. Following the original work of Pandey *et al.* (1980*a*), Kabra *et al.* (1988) also assumed that the layer displacement faults maintain a minimum separation of three layers as required for the transformation of the $2H$ structure into $6H$. The main finding of this work was that the transformation is arrested when 0.276 of the $2H$ layers get faulted, in marked contrast to the predictions of the sequential model which permits completion of the transformation when one third of the layers are faulted. Kabra *et al.* (1988) calculated the intensity distribution along $\mathbf{c}^*$ for the arrested state using the sequential model, taking $6H$ as the reference state. The intensity distribution so obtained was shown to be quite different from that obtained by Pandey *et al.* (1980*c*) using $2H$ as the reference state for the arrested state. Since both calculations were performed using the sequential model taking either $2H$ or $6H$ as the reference state, it was not possible to decide the correctness of one over the other. Also, no attempt was made to verify whether the diffraction effects predicted on the basis of the sequential model will remain valid for the random space model for the intermediate states of transformations prior to the arrested state.

In the present work, computer simulation studies on the $2H$ to $6H$ transformation by the insertion of layer displacement faults in a random space are considered under the assumption that the faults maintain a minimum separation of three layers so as to give rise to the $6H$ structure. It is shown that the numerically computed intensity distribution corresponding to the arrested state in the random space model is significantly different from those predicted by Pandey *et al.* (1980*a*) for the same equivalent sequential fault probability for the layer displacement faults. The numerically computed intensity for the arrested state is, however, found to be in agreement with those obtained by Kabra *et al.* (1988) taking $6H$ as the reference state. It is shown that, for the intermediate states of transformation prior to arrest, the discrepancy between the simulation results and those given by Pandey *et al.* (1980*a*) is small and is negligible for the very early stages of transformation.

2. Pair correlations and diffracted intensities: general considerations

For the numerical computation of diffracted intensities corresponding to the random space model, we have made use of a general formulation originally given by Wilson (1942) and later presented by Holloway (1969) in a more useful form.

Consider a stack of N close-packed layers labelled as $j = 0$ to $N - 1$. Let F_j be the layer form factor for the jth layer. The resultant diffracted amplitude, G, from such a stack of layers can be written as

$$G = (1/N)\{F_0 + F_1 \exp(-i\varphi) + \ldots + F_j \exp(-ij\varphi) + \ldots + F_{N-1} \exp[-i(N-1)\varphi]\}, \quad (1)$$

where φ is the phase difference between rays diffracted from the origins of rhombic unit cells in the adjacent close-packed layers. The diffracted intensity is given by

$$\begin{aligned} GG^* &= (1/N^2)[F_0F_0^* + F_1F_1^* + \ldots + F_{N-1}F_{N-1}^*] \\ &\quad + (1/N^2)\sum_j \sum_m [F_j F_{j+m}^* \exp(im\varphi) \\ &\quad + F_{j+m}F_j^* \exp(-im\varphi)] \\ &= 1/N + \sum_{m=1}^{N-1} [(N-m)/N^2][J_m \exp(im\varphi) \\ &\quad + J_m^* \exp(-im\varphi)], \end{aligned} \quad (2)$$

where $J_m = \langle F_j F_{j+m}^* \rangle$ is the average spatial correlation between the form factor of the jth close-packed layer and the complex conjugate of the form factor for the $(j+m)$th layer. It is easy to see that $J_m = \langle F_j^* F_{j+m} \rangle = \langle F_j F_{j+m}^* \rangle = J_m^*$, where * denotes a complex conjugation operation. Writing the real and imaginary parts of J_m as

$$J_m = J_m' + iJ_m'', \quad (3)$$

(2) can be expressed as

$$\begin{aligned} GG^* &= (1/N^2)\{N + 2(N-1)J_1' \cos\varphi + \ldots \\ &\quad + 2(N-m)J_m' \cos m\varphi + \ldots \\ &\quad + 2J_{(N-1)}' \cos[(N-1)\varphi] - 2(N-1)J_1'' \sin\varphi - \ldots \\ &\quad - 2(N-m)J_m'' \sin m\varphi - \ldots \\ &\quad - 2J_{(N-1)}'' \sin[(N-1)\varphi]\} \\ &= (1/N) + 2\sum_{m=1}^{N-1}[(N-m)/N^2][J_m' \cos m\varphi \\ &\quad - J_m'' \sin m\varphi]. \end{aligned} \quad (4)$$

If the origin is chosen on an A-type site in a close-packed layer, the coordinates of B- and C-type sites in the nth layer with respect to the $2H$ unit cell can be written as $(1/3, -1/3, nz/2)$ and $(-1/3, 1/3, nz/2)$, respectively. The layer form factors (relative to the atomic scattering factor) for A-, B- and C-type layers will thus be

$$\begin{aligned} F_A &= 1, \\ F_B &= \exp[2\pi i(H-K)/3], \\ F_C &= \exp[-2\pi i(H-K)/3], \end{aligned} \quad (5)$$

where $HK.L$ are the Miller–Bravais indices referring to the $2H$ unit cell. Assuming that the spacing between close-packed layers is not affected by faulting, we can write

$$\varphi = \pi h_3, \quad (6)$$

where h_3 is continuous variable along $\mathbf{c}^*$. Let w_A, w_B and

w_C be the probabilities of finding A-, B- and C-type layers in any arbitrary region of the crystal and $p_A(m)$, $p_B(m)$, $p_C(m)$ be the probabilities of the mth layer being in A, B and C orientations. Thus, $\langle F_j F^*_{j+m}\rangle$ can be written as

$$\begin{aligned}\langle F_j F^*_{j+m}\rangle &= w_A p_A(m) F_A F^*_A + w_B p_B(m) F_B F^*_B + w_C p_C(m) F_C F^*_C \\ &\quad + w_A p_B(m) F_A F^*_B + w_B p_C(m) F_B F^*_C + w_C p_A(m) F_C F^*_A \\ &\quad + w_A p_C(m) F_A F^*_C + w_B p_A(m) F_B F^*_A + w_C p_B(m) F_C F^*_B \\ &= [w_A p_A(m) + w_B p_B(m) + w_C p_C(m)] + [w_A p_B(m) \\ &\quad + w_B p_C(m) + w_C p_A(m)] \exp[-2\pi i(H-K)/3] \\ &\quad + [w_A p_C(m) + w_B p_A(m) + w_C p_B(m)] \\ &\quad \times \exp[2\pi i(H-K)/3]. \end{aligned} \tag{7}$$

At this stage, it is useful to define pair correlation functions $P(m)$, $Q(m)$ and $R(m)$ that give the probabilities of finding A–A, B–B, C–C; A–B, B–C, C–A and A–C, C–B, B–A pairs of layers with m-layer separations, respectively. Equation (7) thus simplifies to

$$J_m = \langle F_j F^*_{j+m}\rangle = P(m) + Q(m)\exp(-i\theta) + R(m)\exp(i\theta), \tag{8}$$

where $\theta = 2\pi(H-K)/3$. It is evident from the above expression that reflections with $H - K = 0 \bmod 3$ will not be affected by faulting. Separating the real and imaginary parts of (8), we get

$$J'_m = P(m) + [Q(m) + R(m)]\cos\theta \tag{9}$$

$$J''_m = -[Q(m) - R(m)]\sin\theta. \tag{10}$$

By substituting (9) and (10) into (4), we obtain an intensity expression in terms of $P(m)$, $Q(m)$ and $R(m)$. Thus, calculation of the intensity distribution from a faulted $2H$ crystal reduces to the determination of $P(m)$, $Q(m)$ and $R(m)$. For periodic close-packed structures, $P(m)$, $Q(m)$ and $R(m)$ have got fixed periodically varying values as shown in Figs. 1 and 2 for $2H$ ($AB\ldots$) and $6H$ ($ABCACB\ldots$) structures, respectively. For $2H$, $P(m)$ has values 1 and 0 for $m = 0 \bmod 2$ and $1 \bmod 2$, respectively. For the perfect $6H$, $P(m)$ takes values 1, 0, 1/3, 1/3, 1/3, 0 for $m = 0, 1, 2, 3, 4$ and $5 \bmod 6$, respectively.

3. Pair correlations for the random space model

For the simulation of the $2H$ to $6H$ transformation involving statistical insertion of layer displacement faults using the random space model, we started with a stack of 1200 layers arranged in the AB, $AB\ldots$ or $2H$ manner. In the simulation process, the random selection of layer sites for faulting was made using integer pseudo-random numbers uniformly distributed in the interval [1, 1200]. Each time a layer site was selected for faulting using integer random numbers, the orientation of the selected layer was changed from A/B to C. In order to maintain a minimum separation of three layers between two contiguous layer displacement faults (a requirement for the $6H$ structure to result), two layer sites on either side of a faulted layer were blocked from faulting. Thus, before each insertion of a fault, it is necessary to check whether a randomly selected site can be accepted for faulting or not. The process of random site selection, faulting and blocking of two layer sites on either side of the fault was continued until no more faults could be

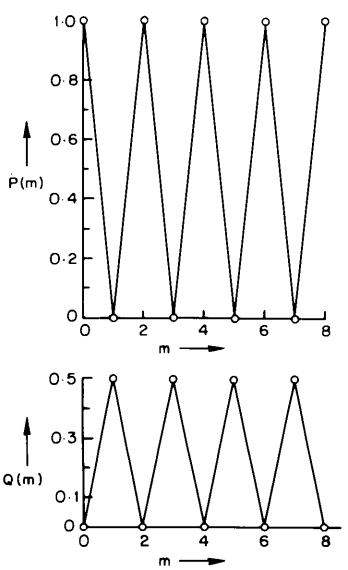

Fig. 1. Pair correlations, $P(m)$ and $Q(m)$, for the perfect $2H$ structure. The probabilities, $P(m)$ and $Q(m)$, are defined only for integer m and the lines between the points are drawn as a guide to the eye.

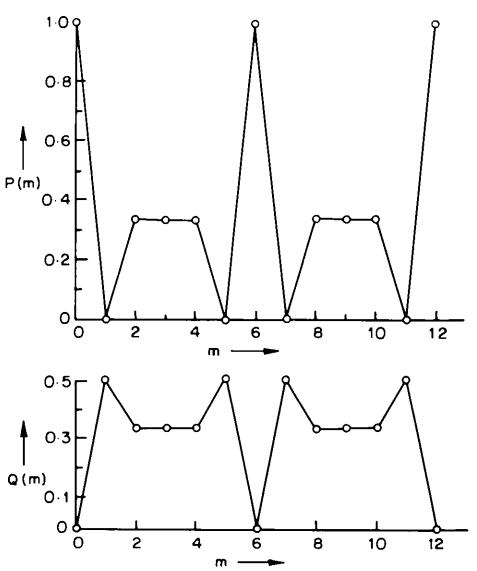

Fig. 2. Pair correlations, $P(m)$ and $Q(m)$, for the perfect $6H$ structure.

inserted. It was found that transformation comes to a halt after the fraction of faulted layers $f = 0.276$.

Using simulated configurations, we have numerically computed $P(m)$, $Q(m)$ and $R(m)$ for the intermediate and the arrested states of transformation. In order to get rid of the boundary and statistical fluctuation effects, it was found sufficient to average these quantities over 1000 configurations, *i.e.* 1000 repeats of the simulation with different random number seeds for a stack of 1200 layers.

Fig. 3 depicts the evolution of $P(m)$ and $Q(m)$ for $f = 0.083$, 0.187 and 0.276, where f is the fraction of faulted layers. It is related to the sequential fault probability α through the following expression (Kabra *et al.*, 1988):

$$f = \alpha/(1 + 2\alpha), \tag{11}$$

The most notable feature in Fig. 3 is the persistence of the $2H$-like long-range ordering throughout the transformation up to the point of arrest. However, the amplitudes of $P(m)$ and $Q(m)$ decrease with respect to the starting value for the perfect $2H$ as the transformation progresses. It is intriguing to note that although long-range $2H$-like ordering persists, the short-range correlations do not correspond to any periodic structure including the $2H$ and $6H$ structures, as can be seen by comparing Fig. 3 with Figs. 1 and 2. The mean $6H$ domain size in the arrested configuration is found to be around nine layers. Since the concept of unit cell for the average structure is valid if the $6H$ unit cell could repeat itself at least once, *i.e.* if the mean domain size is over 12 layers, an average domain size of around nine layers confirms the lack of short-range translational ordering. Thus, the arrested state has long-range ordering without short-range translational correlations (Kabra & Pandey, 1988).

4. Diffracted intensity for the random space model

Let P_e and P_o be the values to which $P(m)$ will converge beyond $m = m'$ for even and odd values of m, respectively [m' is that value of m after which there is no change in $P(m)$ in Fig. 3]. Here, $m' = 5$, 7 and 11 for $f = 0.083$, 0.187 and 0.276, respectively. Similarly, one can obtain Q_e, R_e and Q_o, R_o to which $Q(m)$ and $R(m)$ will converge. Since $Q(m)$ is found to be equal to $R(m)$ beyond m', J''_m given by (10) will be zero for $m > m'$. Further, since $P(m) + Q(m) + R(m) = 1$, $Q_{e/o} = (1/2)[1 - P_{e/o}]$. Thus, J'_m in (9) for $m \geq m'$ will be given by (for reflections with $H - K = \pm 1 \bmod 3$):

$$J'_m = \begin{cases} [3P_e - 1]/2 & \text{for } m \text{ even} \\ [3P_o - 1]/2 & \text{for } m \text{ odd.} \end{cases}$$

We can now split the summation over m in (4) into two parts. In the first part, summation over m extends up to m' only, whereas in the second part the summation is for $m > m'$. Thus, (4) becomes

$$\begin{aligned} I(h_3) &= GG^* \\ &= (1/N) + \sum_{m=1}^{m'} [2(N - m)/N^2] \\ &\quad \times [J'_m \cos m\varphi - J''_m \sin m\varphi] \\ &\quad + \sum_{m=m'+1}^{N-1} [2(N - m)/N^2] J'_m \cos m\varphi. \end{aligned} \tag{12}$$

The second summation in the above expression can be further split into two parts depending on whether m is even or odd. Taking m' as odd and N as even numbers, we can write $m = 2p$ or $2p + 1$ for $m > m'$. Thus, (12)

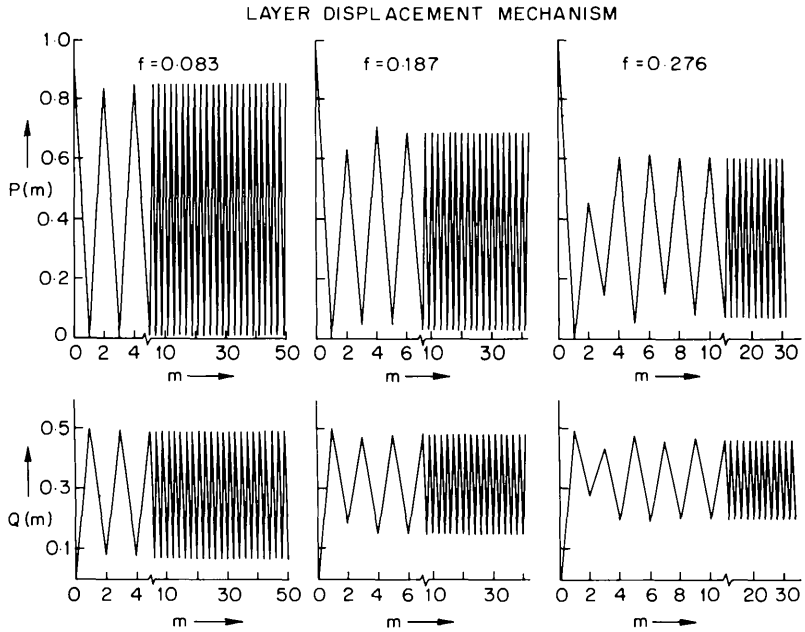

Fig. 3. Numerically computed pair correlations, $P(m)$ and $Q(m)$, corresponding to $f = 0.083$, 0.187 and 0.276 obtained by simulation. The abscissa scale for values of $m < m'$ has been enlarged to aid in detecting the small variation in $P(m)$ and $Q(m)$.

takes the form

$$I(h_3) = (1/N) + \sum_{m=1}^{m'} [2(N-m)/N^2] \times [J'_m \cos m\varphi - J''_m \sin m\varphi] + [(3P_e - 1)/2] \times \sum_{p=(m'+1)/2}^{(N-2)/2} [2(N-2p)/N^2] \cos 2p\varphi + [(3P_o - 1)/2] \sum_{p=(m'+1)/2}^{(N-2)/2} [2(N-2p-1)/N^2] \times \cos(2p+1)\varphi. \quad (13)$$

Adding and subtracting

$$[(3P_e - 1)/2] \sum_{p=1}^{(m'-1)/2} [2(N-2p)/N^2] \cos 2p\varphi$$

and

$$[(3P_o - 1)/2] \sum_{p=0}^{(m'-1)/2} [2(N-2p-1)/N^2] \cos(2p+1)\varphi$$

in (13) we get

$$I(h_3) = (1/N) + \sum_{m=1}^{m'} [2(N-m)/N^2] \times [J'_m \cos m\varphi - J''_m \sin m\varphi] + [(3P_e - 1)/2] \times \sum_{p=1}^{(N-2)/2} [2(N-2p)/N^2] \cos 2p\varphi + [(3P_o - 1)/2] \sum_{p=0}^{(N-2)/2} [2(N-2p-1)/N^2] \times \cos(2p+1)\varphi - [(3P_e - 1)/2] \times \sum_{p=1}^{(m'-1)/2} [2(N-2p)/N^2] \cos 2p\varphi - [(3P_o - 1)/2] \sum_{p=0}^{(m'-1)/2} [2(N-2p-1)/N^2] \times \cos(2p+1)\varphi. \quad (14)$$

On simplification, this reduces to

$$I(h_3) = (1/N^2)\Big\{[3N(1-P_e)/2] + \sum_{p=1}^{(m'-1)/2} (N-2p) \times \{3[P_e(2p) - P_e] \cos 2p\varphi - 2J''_{2p} \sin 2p\varphi\} + \sum_{p=0}^{(m'-1)/2} (N-2p-1) \times \{3[P_o(2p+1) - P_o] \cos(2p+1)\varphi - 2J''_{2p+1} \times \sin(2p+1)\varphi\} + [(\sin^2(N/2)\varphi)/\sin^2\varphi] \times [(3P_e - 1) + (3P_o - 1)\cos\varphi]\Big\}. \quad (15)$$

$P_e(2p)$, P_e, $P_o(2p+1)$ and P_o were determined by averaging over 1000 configurations for $f = 0.083$, 0.187 and 0.276, corresponding to two intermediate states of transformation and the arrested state. These values were then substituted into (15) to obtain the intensity distributions along $\mathbf{c}^*$.

Fig. 4 shows the intensity distributions along $\mathbf{c}^*$ for the two intermediate states and the arrested state. The origins of the second and third curves have been shifted for the sake of clarity. Ideally, $2H$ reflections appear at $h_3 = 0 \bmod 2$ and $\pm 1 \bmod 2$ positions. It is evident from Fig. 4 that the reflections at $h_3 = 0 \bmod 2$ and $\pm 1 \bmod 2$, corresponding to the $2H$ positions, continue to be represented by sharp δ peaks although their weights keep on decreasing with increasing fraction of faulted layers. The two summation terms in (15) give rise to continuous diffuse streaks along $\mathbf{c}^*$, which, with increasing fraction of faulted layers, takes the shape of diffuse elongated spots approximately midway between the $2H$ positions. At the point of arrest, this diffuse reflection shows shoulders near $h_3 = \pm\frac{1}{3} \bmod 2$ positions and a prominent peak near $h_3 = \pm\frac{2}{3} \bmod 2$ positions. Also, the weight of the δ peak at $h_3 = 0 \bmod 2$ becomes vanishingly small. The disappearance of the peak at $h_3 = 0 \bmod 2$, formation of shoulders near $h_3 = \pm\frac{1}{3} \bmod 2$, and the diffuse peaks near $h_3 = \pm\frac{2}{3} \bmod 2$ positions are the signatures of the $6H$-like correlations in the arrested configuration.

5. Comparison with the predictions of the sequential model and experimental observations

We will now compare the numerically computed intensity distributions for the random space model with those expected on the basis of the sequential model developed by Pandey *et al.* (1980*a*). The continuous curves in Fig. 4 show the results for the sequential model while the dotted curves correspond to the random space

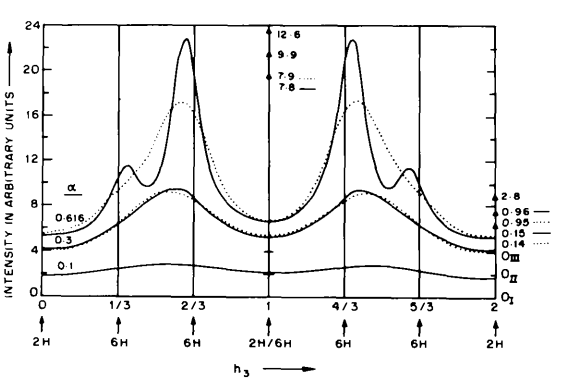

Fig. 4. Intensity distributions along $\mathbf{c}^*$ corresponding to $f(\alpha) = 0.083\,(0.1)$, $0.187\,(0.3)$ and $0.276\,(0.616)$ of the $2H$ to $6H$ transformation occurring by the layer-displacement mechanism. Dotted curves correspond to the random space model and continuous curves correspond to the sequential model. For $\alpha = 0.1$ ($f = 0.083$), the two sets of curves coincide exactly.

model for the layer displacement mechanism. It is evident from Fig. 4 that the $2H$ reflections at $h_3 = 0$, $\pm 1 \bmod 2$ positions continue to be represented by sharp δ peaks in both the models. The weights attached to these δ peaks are also in broad agreement for the two models. Furthermore, the development of diffuse elongated spots midway between the $2H$ reflections during the early stages of transformation is also common to both the models. However, for $f = 0.276$, for which the random space model predicts arrest, the intensity distributions for the two models are in considerable disagreement. The sequential model predicts the splitting of the diffuse elongated spots between the $2H$ reflections into pairs of distinct reflections approaching $h_3 = \pm\frac{1}{3} \bmod 2$ and $\pm\frac{2}{3} \bmod 2$ positions of $6H$. According to the random space model, the diffuse elongated spots do not split into pairs of distinct reflections. There is, of course, a shoulder near $h_3 = \pm\frac{1}{3} \bmod 2$ positions, which is the only signature of the development of $6H$-like ordering.

For SiC-$2H$ crystals undergoing transformation above 1873 K, it has been observed that: (i) the $10.L$ reflections with $L = 0$, $1 \bmod 2$ continue to remain unbroadened throughout the transformation although the intensity of the $L = 0 \bmod 2$ reflections decreases until it merges with the streak; (ii) diffuse elongated spots midway between the $L = 0 \bmod 2$ and $L = 1 \bmod 2$ reflections appear in the course of transformation; and (iii) this diffuse spot does not split into two distinct reflections near $L = \pm\frac{1}{3}$, $\pm\frac{2}{3} \bmod 2$ position characteristic of the $6H$ structure (Pandey *et al.*, 1980*c*). The observations (i) and (ii) are in agreement with the predictions of the sequential as well as the random space models. However, the experimentally observed arrest of the transformation, as indicated by the persistence of the diffuse elongated spots between the $2H$ reflections, can be rationalized in terms of the random space model only since the sequential model predicts eventual completion of the transformation. As mentioned in §3, the arrested state has features of a long-range-ordered phase without short-range translational correlations (Kabra & Pandey, 1988).

6. Discussion

The disagreement between the intensity distributions for the layer displacement mechanism, as predicted on the basis of sequential and random space models for the arrested state, is due to imperfect modelling of the situation by Pandey *et al.* (1980*a*) in terms of the sequential process. In the model employed by Pandey *et al.* (1980*a*), if a layer displacement fault occurs after a 0- or 1-type layer, which is preceded by another fault on the last but two layers, it implies continuation of the $6H$ sequence with probability α. On the other hand, non-occurrence of a fault (probability $1 - \alpha$) in the above situation will lead to interfaces. In the random space model, interfaces resulting from faults occurring at four- and five-layer separations cannot be eliminated because of the minimum separation requirement between two neighbouring layer displacement faults. As a result, the arrested state contains layer displacement faults at three-, four- and five-layer separations, of which only the three-layer separation leads to the $6H$ structure. The interfaces resulting from layer displacement faults occurring at four- and five-layer separations are $I_{2,1}$- and $I_{2,5}$-type intrinsic faults in $6H$ (Pandey, 1984), which are known to give rise to different diffraction effects (Pandey & Krishna, 1976). As shown by Kabra *et al.* (1988), the fault probabilities for these two types of interface deduced from correct sequential modelling of the arrested state are $\alpha_{21} = 0.18$ and $\alpha_{25} = 0.28$. In the sequential analogue of the arrested state in terms of the model considered by Pandey *et al.* (1980*a*), $\alpha_{21} = \alpha_{25} = (1 - \alpha) = 0.38$. The discrepancy between the predicted intensity distributions for the random space and sequential models cannot therefore be resolved unless due consideration to every distinguishable event, such as stacking faults occurring in the present case at four- and five-layer separations, is given. In fact, the intensity distribution calculated by considering the arrested state as a faulted $6H$ crystal with $\alpha_{21} = 0.18$ and $\alpha_{25} = 0.28$ [see Fig. 5 of Kabra *et al.* (1988)] is in agreement with those predicted in the present paper on the basis of the random space model. It is thus evident that a correct sequential model for the $2H$ to $6H$ transformation should be based on three probabilities corresponding to faults occurring at three-, four- and five-layer separations. However, for such a model to be useful, the determination of the three sequential fault probabilities has to be done using simulated configurations. Once these probabilities have been determined correctly, the subsequent intensity calculation can, in principle, be carried out analytically. However, the utility of the sequential model will still remain restricted because of its dependence on the simulation approach for the determination of realistic values of the fault probabilities that form the most essential ingredient for any intensity calculation. Furthermore, this type of calculation will be applicable for the arrested state only and have restricted validity.

7. Concluding remarks

The sequential model, based on the Markovian chain approach for the calculation of diffuse intensity distribution due to layer displacement faults, is physically unrealistic for crystals undergoing a $2H$ to $6H$ phase transformation through a non-random insertion of stacking faults. Since the faults bringing about such transformations maintain certain minimum separation so as to give rise to the product phase, the transformation gets arrested well before its completion. In such situations, the diffuse intensity distributions for the intermediate states of transformation can be conveniently obtained numerically using the computer simulation

approach outlined in this paper. The predicted diffraction effects based on the computer simulation approach do not affect the main conclusion of Pandey *et al.* (1980*a*) that the 2*H* to 6*H* transformation in SiC occurs by the layer displacement mechanism.

References

AHLERS, M. & PLEGRINA, J. L. (1992). *Acta Met. Mater.* **40**, 3213–3220.
CARDELLINI, F. & MAZZONE, G. (1993). *Philos. Mag.* A**67**, 1289.
DEMIN, S. A., NEKRASOV, A. A. & USTINOV, A. I. (1993). *Acta Met. Mater.* **41**, 2091–2095.
FREY, F. & BOYSEN, H. (1981). *Acta Cryst.* A**37**, 819–826.
HITZENBERGER, C., KARNTHALER, H. P. & KORNER, A. (1985). *Acta Met. Mater.* **33**, 1293–1305.
HOLLOWAY, H. (1969). *J. Appl. Phys.* **40**, 4313–4321.
JAGODZINSKI, H. (1971). *Kristallogr.* **16**, 1235–1246.
JEPPS, N. W. & PAGE, T. F. (1980). *J. Microsc.* **119**, 177–188.
KABRA, V. K. & PANDEY, D. (1988). *Phys. Rev. Lett.* **61**, 1493–1496.
KABRA, V. K., PANDEY, D. & LELE, S. (1986). *J. Mater. Sci.* **21**, 1654–1666.
KABRA, V. K., PANDEY, D. & LELE, S. (1988). *J. Appl. Cryst.* **21**, 935–942.
KRISHNA, P. & MARSHALL, R. C. (1971*a*). *J. Cryst. Growth*, **9**, 319–325.
KRISHNA, P. & MARSHALL, R. C. (1971*b*). *J. Cryst. Growth*, **11**, 147–150.
MINAGAWA, T. (1978). *J. Appl. Cryst.* **11**, 243–247.
MUTO, S., VAN TENDELOO, G. & AMELINCKX, S. (1993). *Philos. Mag.* B**67**, 443–463.
NIKOLIN, B. I., BABKEVICH, A. YU., IZDKOVSKAYA, T. V. & PETROVA, S. N. (1993). *Acta Met. Mater.* **41**, 513–515.
OGBUJI, L. U., MITCHELL, T. E. & HEUER, A. H. (1981). *J. Am. Ceram. Soc.* **64**, 91–99.
PANDEY, D. (1976). PhD thesis, Banaras Hindu Univ., India.
PANDEY, D. (1984). *Acta Cryst.* B**40**, 567–569.
PANDEY, D., KABRA, V. K. & LELE, S. (1986). *Bull. Miner.* **109**, 49–67.
PANDEY, D. & KRISHNA, P. (1976). *Acta Cryst.* A**32**, 488–492.
PANDEY, D. & KRISHNA, P. (1982). *Current Topics in Materials Science*, Vol. 9, edited by E. KALDIS, pp. 415–491. Amsterdam: North-Holland.
PANDEY, D. & KRISHNA, P. (1983). *Prog. Cryst. Growth Charact.* **7**, 213–252.
PANDEY, D. & LELE, S. (1986). *Acta Metall.* **34**, 405–413, 415–424.
PANDEY, D., LELE, S. & KRISHNA, P. (1980*a*). *Proc. R. Soc. London Ser. A*, **369**, 435–449.
PANDEY, D., LELE, S. & KRISHNA, P. (1980*b*). *Proc. R. Soc. London Ser. A.* **369**, 451–461.
PANDEY, D., LELE, S. & KRISHNA, P. (1980*c*). *Proc. R. Soc. London Ser. A*, **369**, 463–477.
SEBASTIAN, M. T., PANDEY, D. & KRISHNA, P. (1982). *Phys. Status Solidi A*, **71**, 633–640.
WILSON, A. J. C. (1942). *Proc. R. Soc. London Ser. A*, **180**, 277–285.

Acta Cryst. (1995). A**51**, 335–343

Arithmetic Properties of Module Directions in Quasicrystals, Coincidence Modules and Coincidence Quasilattices

BY O. RADULESCU

Laboratoire de Recherche sur les Matériaux, Université Marne-la-Vallée, Bâtiment IFI, 2 rue de la Butte Verte, 93166 Noisy-le-Grand, France

AND D. H. WARRINGTON*

Department of Engineering Materials, University of Sheffield, PO Box 600, Sheffield S1 4DH, England

(*Received* 20 *June* 1994; *accepted* 13 *October* 1994)

Abstract

Two new concepts are introduced that are useful for the classification of grain boundaries of quasicrystals: the coincidence module and the coincidence quasilattice. Related to these concepts is the distribution of lengths in different directions of a quasicrystalline module, which, for quasicrystals whose geometry is based on quadratic irrational numbers, is determined by an arithmetic form of the type $sx^2 - y^2$, where s is a square-free integer.

1. Introduction

Rotation of two identical lattices with respect to each other leads, for some special values of the rotation angle, to coincidences of the vertices. In the case of normal crystals, these coincident vertices form the coincidence-site lattice (CSL) (Friedel, 1964; Warrington & Buffalini, 1971; Grimmer, Bollmann & Warrington, 1974). The CSL is important in crystallography because it allows a nontrivial classification of grain boundaries and because small-unit-cell CSL grain boundaries seem to be energetically favoured (see, for instance, Sutton & Balluffi, 1987).

It has been shown (Warrington, 1992, 1993*a*,*b*) that coincidences of the vertices appear also in quasicrystalline tilings. We give here some geometrical tools needed for the study of coincidences in quasicrystals. We first introduce in a unifying perspective the projection schemes for quasicrystals based on quadratic irrationalities, then discuss the concepts of the coincidence module

* Honorary reader.